Engineered Science

RESEARCH PAPER

View Article Online

A Highly Porous Polyaniline-Graphene Composite Used for Electrochemical Supercapacitors

Xiaomin Li, Wen Zhao, Rui Yin, Xiaoshuai Huang and Lei Qian*

A polyaniline (PANI)-porous graphene (PGR) hybrid material with high capacitive performance was synthesized through electropolymerization of aniline on the PGR. The microstructure and morphologies of the PANI-PGR were characterized by field emission scanning electron microscopy, while electrochemical behaviors were measured by cyclic voltammetry and galvanostatic charge-discharge. The effects of aniline and PGR concentrations and polymerization cycles on electrochemical performances of the PANI-PGR were investigated. The results demonstrated that the prepared $PANI_{0.05}$-$PGR_{1.25}$-15 (0.05 M aniline, 1.25 mg·ml^{-1} PGR and 15 polymerization cycles) showed the highest specific capacitance of 1209 F·g^{-1} at 0.2 A·g^{-1}. The specific capacitance of the obtained PANI-PGR was higher compared with other PANI materials, such as graphene (GR)-wrapped PANI nanofiber, single walled carbon nanotube/PANI, and GR-PANI nanoworm composites. The $PANI_{0.05}$-$PGR_{1.25}$-15 also displayed good cycle stability, retaining 92% of the initial capacitance after 1000 cycles of charge-discharge. The excellent capacitive properties were attributed to large specific surface area of the PGR and good pseudocapacitive properties of PANI.

Keywords: Polyaniline; Supercapacitor; Porous graphene; Electropolymerization

Received 21st June 2018, Accepted 29th July 2018

DOI: 10.30919/es8d743

1. Introduction

Nowadays, a large number of researchers have paid tremendous attention to supercapacitors (SCs) owing to their especially long cycle-life, remarkable charge and discharge performance, reversible charge storage mechanism, and high power density.[1] Electrode materials have a critical impact on the properties of SCs, so it is very important and necessary to prepare high-performance electrode materials for their applications.[2–9]

It is well known that the conductive polymer is an outstanding candidate of electrode material for SCs because of its excellent capacitive property. Among the conductive polymers, polyaniline (PANI) has shown great potential due to its rapid charge and discharge property, unique deposing/posing process, remarkable conductivity in doped states and extremely superior specific capacitance.[10–14] However, there are some shortcomings for PANI as electrode materials hindering its application in SCs. For instance, PANI has poor cycle stability resulting from the significant volume shrinkage and expansion in the repetitive redox process.[15] In order to overcome these shortcomings, an effective method is combining PANI with other conductive materials to prepare hybrid materials. Carbon material is considered as an excellent choice due to its instinct good cycle stability.[16] Many composites of carbon materials and PANI have been reported such as PANI-carbon nanotube (CNT),[16–26] PANI-carbon aerogels,[27] PANI-activated carbon,[28–32] and PANI-graphene.[33–35] Among these composites, graphene (GR) is shown to be an excellent material when combining with PANI, owing to its unique two dimensional monolayer structure, special sp^2 hybrid pattern, extremely large surface area and high electron transfer activity.[36,37] For example, the synthesized hierarchical GR-PANI nanoworm composites gave a specific capacitance of 488 F·g^{-1} at 0.5 A·g^{-1}.[38] Flexible PANI-GR nanofiber composite films were also produced by vacuum filtration of the mixed dispersions of GR and PANI nanofibers, and the maximum specific capacitance reached 210 F·g^{-1} at 0.3 A·g^{-1}.[39] The 3D PANI-GR hollow hybrid microspheres provided a specific capacitance of 331 F·g^{-1} at 1 A·g^{-1}.[40] But due to the GR agglomeration resulting from the interaction of π-π bond and van der Waals force between the GR sheets, its specific surface area, loading capacity and electron transfer rate significantly decreased, resulting in poor capacitance performance.[39] To resolve this issue, our group recently reported that porous graphene (PGR) with three-dimensional pores was prepared by freeze-drying.[41,42] Compared with pristine GR, PGR had large surface areas, sufficient activity sites, and efficient diffusion activity. Based on these advantages, we combined PGR with PANI to obtain a high-performance PANI-PGR hybrid material via electropolymerization. The microstructures and morphologies of PANI-PGR were characterized by field emission scanning electron microscopy (FESEM). Electrochemical behaviors were measured by cyclic voltammetry (CV) and galvanostatic

Key Laboratory for Liquid–Solid Structural Evolution and Processing of Materials (Ministry of Education), Shandong University, 17923 Jingshi Road, Jinan 250061, China. E-mail: qleric@sdu.edu.cn

charge-discharge (GCD). The impacts of aniline and PGR concentrations, and polymerization cycles on capacitive performances of the PANI-PGR were investigated.

2. Experimental

2.1. Chemical and reagents

5% Nafion solution was purchased from Sigma-Aldrich. Graphene oxide (GO) was obtained from Nanjing JCNano. Tech.Co., LTD. Aniline was from Sino pharm Group Reagent Co. Ltd. All chemical and reagents were of analytical grade, and water used in the experiment was deionized water.

2.2. Apparatus

Electrochemical workstation (CHI660D) was purchased from Shanghai ChenHua Instrument Co. LTD. Microstructures of materials were characterized by a SU-70 FESEM with an accelerating voltage of 15 kV. The modified glassy carbon electrode was as work electrode (GCE, 3 mm diameter). A platinum wire was used as counter electrode and Ag/AgCl in saturated KCl solution was served as reference electrode.

2.3. Preparation of the PGR modified GCE

PGR was obtained according to our previously reported method.[42] First, 1.0, 1.25, 2.5 and 5 mg PGR was added to 1 ml 0.5 % Nafion solution, respectively. The mixtures were dispersed under ultrasonication to prepare uniform and stable PGR suspensions (1, 1.25, 2.5 and 5 $mg{\cdot}ml^{-1}$). The GCE was polished with some alumina powder on the polished cloth. After that the GCE was cleaned with ethanol and distilled water, respectively, and dried in nitrogen. Finally, the PGR suspension was dropped onto the surface of GCE and dried at room temperature to produce the PGR modified GCE.

2.4. Electropolymerization of aniline on the PGR modified GCE

PANI-PGR hybrid materials obtained from different experimental conditions including aniline concentration, PGR concentration and polymerization cycles are shown in Table 1. The PANI-PGR was synthesized by electropolymerization onto the PGR modified GCE. The electropolymerization was carried out over the range of -0.2-0.8 V with the scanning rate of 100 $mV{\cdot}s^{-1}$ in 0.1 M H_2SO_4 solution with aniline.

Table 1 PANI-PGR hybrid materials obtained from different experimental conditions including aniline concentration, PGR concentration and electropolymerization cycles.

Sample	Aniline concentration (M)	PGR concentration ($mg{\cdot}ml^{-1}$)	Electro-polymerization cycles
$PANI_{0.05}PGR_5$-15	0.05	5	15
$PANI_{0.05}PGR_{2.5}$-15	0.05	2.5	15
$PANI_{0.05}PGR_{1.25}$-15	0.05	1.25	15
$PANI_{0.05}PGR_1$-15	0.05	1	15
$PANI_{0.05}PGR_{1.25}$-5	0.05	1.25	5
$PANI_{0.05}PGR_{1.25}$-10	0.05	1.25	10
$PANI_{0.05}PGR_{1.25}$-20	0.05	1.25	20
$PANI_{0.025}PGR_{1.25}$-15	0.025	1.25	15
$PANI_{0.1}PGR_{1.25}$-15	0.1	1.25	15

The total mass of PANI deposited on the electrode was determined by Faraday's law as the following equation:

$$m = \frac{QM}{zF}$$

where m is the mass of PANI, Q is the quantity of charge loaded, M is the molar mass of the aniline monomer and F is the Faraday constant (96485 $C{\cdot}mol^{-1}$).

2.5. Capacitive performance of PANI-PGR composites

To assess the electrochemical performance of composites, CV and GCD tests were investigated in a 0.1 M H_2SO_4 aqueous solution. The cyclic voltammetry was carried out in the voltage range of -0.2 ~ 0.8 V with the scanning rates from 10 to 100 $mV{\cdot}s^{-1}$. The specific capacitance was calculated by the following equation:

$$C = \frac{\int VdI}{mVv}$$

where m is the mass of gross active material on the electrode, V is the potential range, I indicates the current and v is the scanning rates.

GCD was tested with a potential range of -0.2-0.6 V and the specific capacitance was calculated via the following equation:

$$C = \frac{It}{mV}$$

where C represents specific capacitance, I is discharge current, t indicates discharge time, and m is the mass of gross active material on the electrode.

3. Result and discussion

3.1. Morphologies of the PANI-PGR composites

FESEM was used to examine the morphologies and microstructures of the PANI-PGR and PGR. Fig. 1a gives the image of the resulted PGR and it was found that there were many three-dimensional interlinked pores throughout the PGR. These pores were formed during the following treatment process: when the suspension was rapidly frozen in liquid nitrogen, water in the suspension was condensed into ice crystals at low temperature. After that, the ice crystals were sublimated in vacuum at low temperature and this resulted in three dimensional porous structures. The good porous structure increased the specific surface area and effectively promoted the ion adsorption and diffusion, which was conductive to the enhancement of their capacitance performance. Fig. 1b gives the FESEM image of the $PANI_{0.05}PGR_{1.25}$-15, and extensive membrane-like substances on the PGR surface are clearly observed, indicating that the PANI was obtained by electropolymerization and uniformly distributed on the surface of PGR. In addition, PANI-PGR still kept original porous structures of PGR during the electropolymerization. The FESEM image of the $PANI_{0.05}PGR_{1.25}$-15 at high magnification is shown in Fig. 1c. Compared with the relatively rough surfaces of PGR,

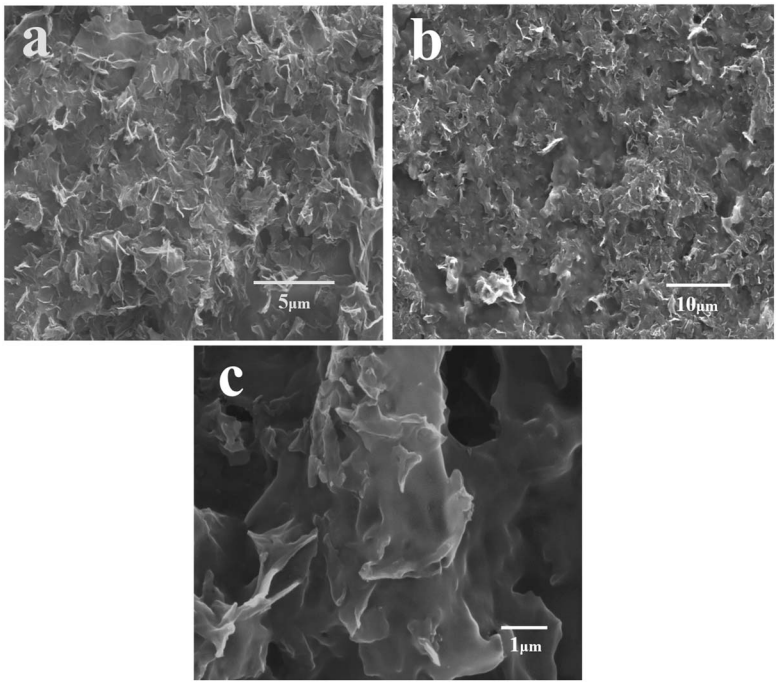

Fig. 1 FESEM images of PGR (a), $PANI_{0.05}PGR_{1.25}$-15 (b) and $PANI_{0.05}PGR_{1.25}$-15 at high magnification (c).

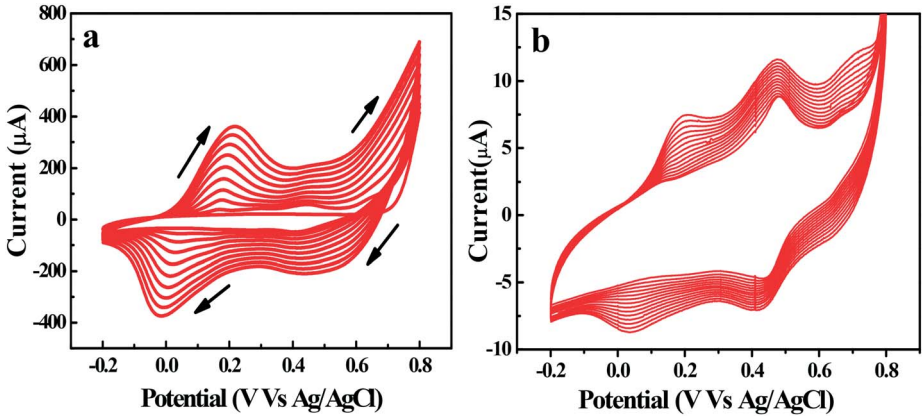

Fig. 2 CV curves of aniline electropolymerization on the PGR modified GCE (a) and the bare GCE (b) at a scanning rate of 100 $mV{\cdot}s^{-1}$ in 0.1 M H_2SO_4.

PANI-PGR had smooth surfaces and some porous structures were filled with the PANI, which further proved the existence of PANI.

3.2. Elctrochemical properties of the PANI–PGR composites

Fig. 2a describes the CV curvs of the aniline electropolymerization process on the PGR modified GCE at 100 $mV{\cdot}s^{-1}$. Two pairs of redox peaks at around 0.1 and 0.45 V were also observed, corresponding to different redox reactions in the electropolymerization process. The electropolymerization of aniline was explained according to the reported literatures.[18,43] First, aniline molecules were oxidized under a certain potential to form cationic free radicals. Then, the cationic radicals combined with each other to form different dimers. Finally, the dimers translated into oligomer, which deposited on the electrode surface to produce the PANI film. With the growth of polymerization cycles, the peak currents gradually increased, indicating that polyaniline films were produced on the PGR modified GCE. Fig. 2b shows the CV curves of electropolymerization process of aniline on the bare GCE at 100 $mV{\cdot}s^{-1}$ in 0.1 M H_2SO_4. In Fig. 2b, two redox peaks appeared and there was no significant difference of the peak position between Fig. 2a and 2b. It indicates the similar redox processes occurred during the electropolymerization. However, the peak currents in Fig. 2a were nearly 50 times as that in Fig. 2b, attributed to the fact that PGR modified GCE possessed better conductivity and more active sites than bare GCE.

The CV curves of $PANI_{0.05}$-15 and $PANI_{0.05}PGR_{1.25}$-15 in 0.1 M H_2SO_4 at a scanning rate of 100 $mV{\cdot}s^{-1}$ are shown in Fig. 3. The area surrounded by the CV curve of $PANI_{0.05}PGR_{1.25}$-15 was larger than that of the $PANI_{0.05}$-15. According to the theory that the area of the CV curve was proportional to the specific capacitance of an electrode,[44] the

result shows that specific capacitance of the $PANI_{0.05}PGR_{1.25}$-15 significantly exceeded that of the $PANI_{0.05}$-15. The reason was that PANI-PGR possessed the three-dimensional interconnected and porous structure, providing large surface areas and accelerating the electron transfer process.

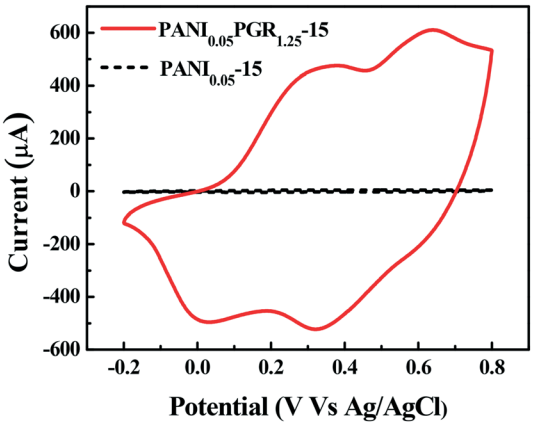

Fig. 3 CV curves of the $PANI_{0.05}$-15 and $PANI_{0.05}PGR_{1.25}$-15 modfied GCE at a scanning rate of 100 mV·s^{-1} in 0.1 M H_2SO_4.

3.3. Supercapacitive performances of the PANI-PGR composites

Different PANI-PGR composites ($PANI_{0.05}PGR_1$-15, $PANI_{0.05}PGR_{1.25}$-15, $PANI_{0.05}PGR_{2.5}$-15, $PANI_{0.05}PGR_5$-15) were prepared and their supercapacitive performances were explored by CV and GCD. CV curves of the $PANI_{0.05}PGR_{2.5}$-15 modified GCE at different scanning rates from 10, 20, 40, 60, 80, 100 mV·s^{-1} in 0.1 M H_2SO_4 are shown in Fig. 4a. Obvious redox peaks were observed, indicating that the specific capacitance mainly resulted from the faradaic mechanism. The first pair of peaks at about 0.1 V resulted from PANI transformed from the reduced polybenzene to emeraldine.[45,46] The second pair of peaks at about 0.5 V was attributed to the emeraldine transforming to aniline in the oxidized state.[47] The lines charts of specific capacitance from the PANI-PGR including various PGR concentration based on CV curves are shown in Fig. 4b. As the concentrations of PGR increased from 1 to 1.25 mg·ml^{-1}, the specific capacitance at a scanning rate of 80 mV·s^{-1} significantly increased from 726.1 to 893.8 F·g^{-1}. However, the specific capacitance reduced gradually when PGR concentration was over 1.25 mg·ml^{-1}, and the corresponding capacitance were 893.8, 436.8 and 244.3 F·g^{-1} for $PANI_{0.05}PGR_{1.25}$-15, $PANI_{0.05}PGR_{2.5}$-15, $PANI_{0.05}PGR_5$-15 at 80 mV·s^{-1}, respectively. It is attributed to the fact that optimized concentration of PGR with good porous structure was conducive to the transmission of electrons. However, the

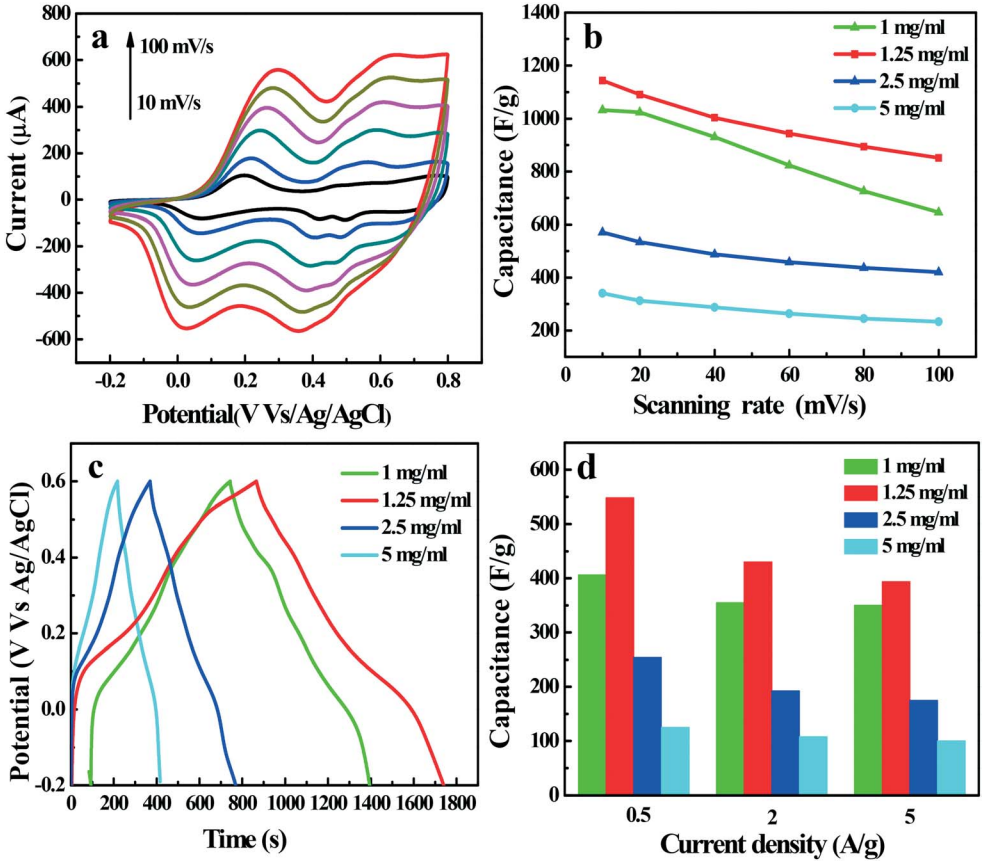

Fig. 4 (a) CV curves of the $PANI_{0.05}PGR_{2.5}$-15 modified GCE at different scanning rates from 10, 20, 40, 60, 80 to 100 mV·s^{-1}, (b) Specific capacitance of the $PANI_{0.05}PGR_1$-15, $PANI_{0.05}PGR_{1.25}$-15, $PANI_{0.05}PGR_{2.5}$-15 and $PANI_{0.05}PGR_5$-15 modified GCE from CV curves at different scanning rates from 10, 20, 40, 60, 80 to 100 mV·s^{-1}, (c) GCD curves of the $PANI_{0.05}PGR_1$-15, $PANI_{0.05}PGR_{1.25}$-15, $PANI_{0.05}PGR_{2.5}$-15 and $PANI_{0.05}PGR_5$-15 modified GCE at 0.5 A·g^{-1}, (d) Specific capacitance of the $PANI_{0.05}PGR_1$-15 $PANI_{0.05}PGR_{1.25}$-15, $PANI_{0.05}PGR_{2.5}$-15 and $PANI_{0.05}PGR_5$-15 modified GCE from GCD at different current density from 0.5, 2 to 5 A·g^{-1}.

excess PGR (2.5 and 5 mg·ml^{-1}) hindered the electron transfer in the interface between the electrode and electrolyte. In addition, the specific capacitance reduced with the scanning rates increased from 10 to 100 mV·s^{-1}. Although the specific capacitance of $PANI_{0.05}$-$PGR_{1.25}$-15 decreased as the scanning rate increased, it was still up to 851 F·g^{-1} even at a high scanning rate of 100 mV·s^{-1}, indicating the remarkable rate performance. GCD curves of the $PANI_{0.05}PGR_1$-15, $PANI_{0.05}PGR_{1.25}$-15, $PANI_{0.05}PGR_{2.5}$-15, $PANI_{0.05}PGR_5$-15 modified GCE at 0.5 A·g^{-1} in 0.1 M H_2SO_4 are also shown in Fig. 4c. All of the charge-discharge curves exhibited obvious voltage platform, indicating their typical pseudocapacitive behaviors, which were consistent with the CV results. And the curves were highly symmetric, indicating good reversibility. It was obvious that the discharge time of $PANI_{0.05}PGR_{1.25}$-15 was longer than that of $PANI_{0.05}PGR_1$-15, $PANI_{0.05}PGR_{2.5}$-15 and $PANI_{0.05}PGR_5$-15, demonstrating that $PANI_{0.05}PGR_{1.25}$-15 exhibited the highest specific capacitance (1209 F·g^{-1} at 0.2 A·g^{-1}). The bar charts of specific capacitance of GCD curves from the PANI-PGR including different PGR concentrations at 0.5, 2 and 5 A·g^{-1} are shown in Fig. 4d. The specific capacitance of $PANI_{0.05}PGR_{1.25}$-15 was the highest among all the samples. When the concentration of PGR increased from 1 to 1.25 mg·ml^{-1}, the specific capacitance changed from 408 to 548 F·g^{-1} at a current density of 0.5 A·g^{-1}. With the concentration of PGR increased from 1.25 to 2.5 and 5 mg·ml^{-1}, the specific capacitance changed from 548 to 254 and 125 F·g^{-1} at 0.5 A·g^{-1}. The specific capacitance exceeded that of other PANI-carbon composite materials, such as GR-wrapped PANI nanofiber composites (250 F·g^{-1}), PANI/single walled carbon nanotube/cloth (410 F·g^{-1}), GR-PANI Nanoworm composites (488 F·g^{-1}) and MWNTs/PANI composite (224 F·g^{-1}) and so on.[38,48–50]

The effect of different aniline concentrations was also studied by CV and GCD. Fig. 5a shows the specific capacitances calculated by CV curves at the scanning rates from 10, 20, 40, 60, 80 to 100 mV·s^{-1} in 0.1 M H_2SO_4. When the concentration of aniline increased from 0.025 to 0.05 M, the specific capacitance increased from 693.9 to 851.5 F·g^{-1} at 100 mV·s^{-1}. However, the specific capacitance decreased to 760.9 F·g^{-1} as the aniline concentration further increased to 0.1 M. The reason was that appropriate increase of the aniline concentration was conductive to specific capacitance due to its inherent good pseudocapacitance properties, while aniline monomers with high concentration formed excessive polyaniline, limiting dramatically the electron transfer. The GCD curves of $PANI_{0.025}PGR_{1.25}$-15, $PANI_{0.05}PGR_{1.25}$-15, $PANI_{0.1}PGR_{1.25}$-15 modified GCE at 5 A·g^{-1} in 0.1 M H_2SO_4 solution are shown in Fig. 5b. Compared with other materials, $PANI_{0.05}PGR_{1.25}$-15 had the long discharge time, representing its optimal capacitance performance. Fig. 5c displayed the specific capacitances of the $PANI_{0.025}PGR_{1.25}$-15, $PANI_{0.05}PGR_{1.25}$-15 and $PANI_{0.1}PGR_{1.25}$-15 calculated from their GCD curves. As the

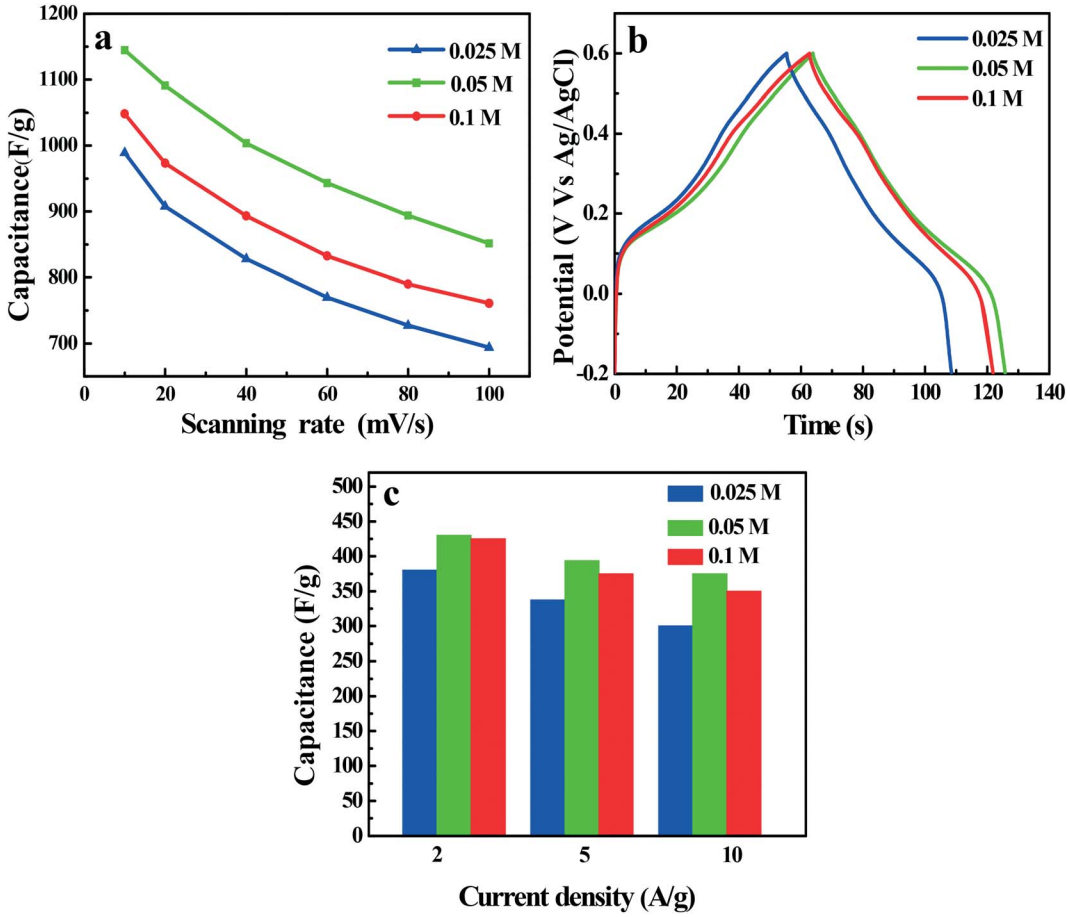

Fig. 5 (a) Specific capacitance of the $PANI_{0.025}PGR_{1.25}$-15, $PANI_{0.05}PGR_{1.25}$-15 and $PANI_{0.1}PGR_{1.25}$-15 modified GCE by CV curves at different scanning rates from 10, 20 40, 60, 80 to 100 mV·s^{-1}, (b) GCD curves of the $PANI_{0.025}PGR_{1.25}$-15, $PANI_{0.05}PGR_{1.25}$-15, $PANI_{0.1}PGR_{1.25}$-15 modified GCE at 5 A·g^{-1}, (c) Specific capacitance of the $PANI_{0.025}PGR_{1.25}$-15, $PANI_{0.05}PGR_{1.25}$-15 and $PANI_{0.1}PGR_{1.25}$-15 modified GCE from GCD at different current density from 2, 5 to 10 A·g^{-1}.

concentration of aniline monomers changed from 0.025, 0.05 to 0.1 M, the discharge time increased first and then decreased. The highest specific capacitance of 430 $F \cdot g^{-1}$ at 2 $A \cdot g^{-1}$ was obtained for $PANI_{0.05}PGR_{1.25}$-15.

In order to study the effect of polymerization cycles, the capacitive properties of $PANI_{0.05}PANR_{1.25}$-5, $PANI_{0.05}PGR_{1.25}$-10, $PANI_{0.05}PGR_{1.25}$-15, $PANI_{0.05}PGR_{1.25}$-20 were investigated in 0.1 M H_2SO_4 from -0.2 to 0.8 V. Fig. 6a gives the line charts of PANI-PGR including different polymerization cycles from the CV curves at different scanning rates from 10, 20, 40, 60, 80 to 100 $mV \cdot s^{-1}$ in 0.1 M H_2SO_4. It was found that when the polymerization cycles were changed from 5, 10 to 15, the specific capacitance of the material increased from 424.7, 779.9 to 1144.74 $F \cdot g^{-1}$ at 10 $mV \cdot s^{-1}$. Whereas the specific capacitance reduced to 716 $F \cdot g^{-1}$ when the polymerization cycles increased to 20. The GCD curves of PANI-PGR from different polymerization cycles at 1 $A \cdot g^{-1}$ in 0.1 M H_2SO_4 solution are also shown in Fig. 6b. When polymerization cycles were less than 15, the discharge time gradually extended with the polymerization cycles, indicating the corresponding specific capacitance increased. However, when the polymerization cycles were increased from 15 to 20, the discharge time decreased significantly. The phenomenon indicated that excessive polymerization cycles had a negative impact on the electrochemical performance of the material. Fig. 6c shows the bar charts of specific capacitance of samples including various polymerization cycles from GCD curves at 1, 5 and 10 $A \cdot g^{-1}$ in 0.1 M H_2SO_4 solution. It was found that when the polymerization cycles were changed from 5, 10 to 15 cycles, the specific capacitance increased from 235, 356 to 500 $F \cdot g^{-1}$ at 1 $A \cdot g^{-1}$. The specific capacitance decreased to 282 $F \cdot g^{-1}$ at 1 $A \cdot g^{-1}$ when polymerization cycles were 20. The reason is ascribed to the fact that as the polymerization cycles were increased, the amount of obtained PANI increased and improved the capacitance performance of composites. However, excess cycles led to a dense polyaniline film on the surface of PGR, which blocked the effective electron transfer and reduced the specific capacitance.

The cycle stability of $PANI_{0.05}PGR_{1.25}$-15 was tested at the current density of 10 $A \cdot g^{-1}$ for 1000 cycles and the corresponding result is shown in Fig. 7. After 1000 cycles, the capacitor retention rate was still around 92%, indicating that the $PANI_{0.05}PGR_{1.25}$-15 exhibited excellent cycle stability.

4. Conclusions

In summary, the PANI-PGR composites have been synthesized via electro polymerization of PANI on the PGR modified GCE. The prepared PGR had appropriate porosity and large specific surface areas, which was conductive to the electropolymerization of PANI on the

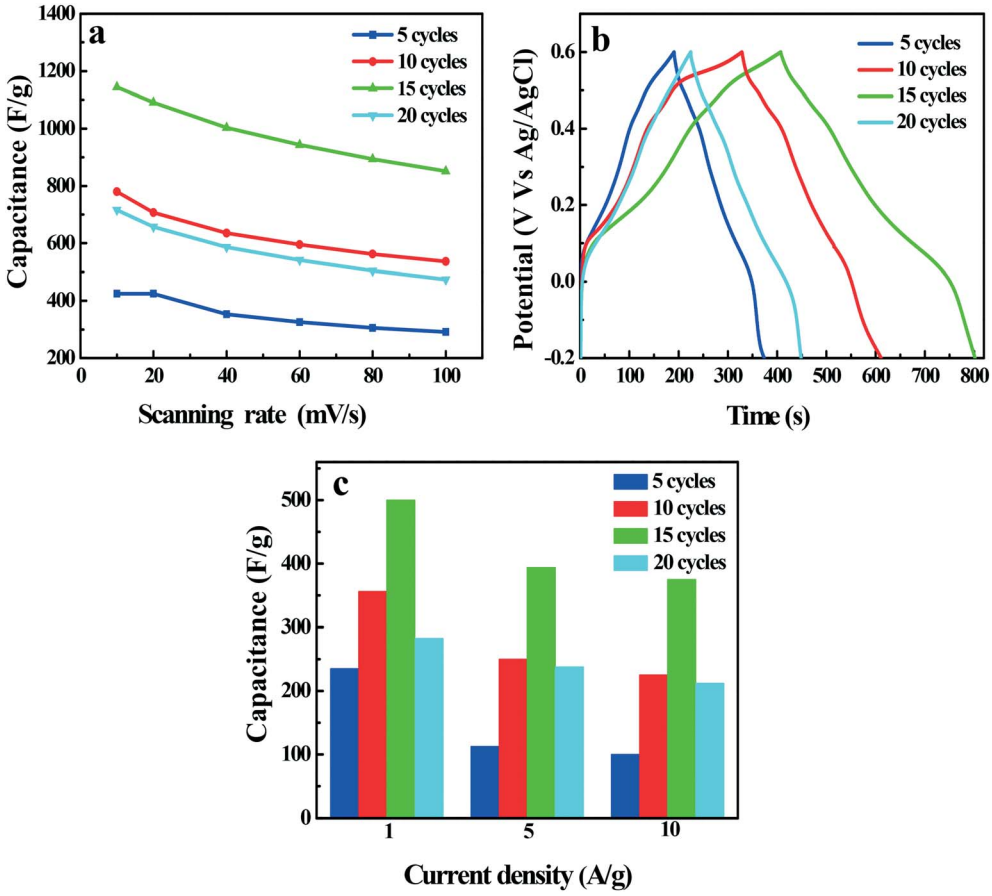

Fig. 6 (a) Specific capacitance of the $PANI_{0.05}PGR_{1.25}$-5, $PANI_{0.05}PGR_{1.25}$-10, $PANI_{0.05}PGR_{1.25}$-15, $PANI_{0.05}PGR_{1.25}$-20 modified GCE by CV curves at different scanning rates from 10, 20, 40, 60, 80 to 100 $mV \cdot s^{-1}$, (b) GCD curves of the $PANI_{0.05}PGR_{1.25}$-5, $PANI_{0.05}PGR_{1.25}$-10, $PANI_{0.05}PGR_{1.25}$-15 and $PANI_{0.05}PGR_{1.25}$-20 modified GCE at 1 $A \cdot g^{-1}$, (c) Specific capacitance of the $PANI_{0.05}PGR_{1.25}$-5, $PANI_{0.05}GR_{1.25}$-10, $PANI_{0.05}GR_{1.25}$-15 and $PANI_{0.05}PGR_{1.25}$-20 modified GCE from GCD at different current density from 1, 5 to 10 $A \cdot g^{-1}$.

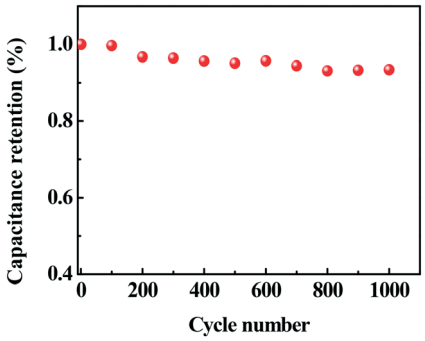

Fig. 7 Cycle stability of th $PANI_{0.05}PGR_{1.25}$-15 modified GCE in 0.1 M H_2SO_4 at the current density of 10 $A{\cdot}g^{-1}$.

PGR modified GCE. The impacts of concentration of aniline and PGR as well as polymerization cycles on electrochemical performances of the PANI-PGR were investigated. The results demonstrate that the prepared $PANI_{0.05}$-$PGR_{1.25}$-15 (0.05 M aniline, 1.25 $mg{\cdot}ml^{-1}$ PGR and 15 polymerization cycles) showed the highest specific capacitance and good cycle stability. The highest specific capacitance reached 1209 $F{\cdot}g^{-1}$ at the current density of 0.2 $A{\cdot}g^{-1}$ and 1144 $F{\cdot}g^{-1}$ at the scanning rates of 10 $mV{\cdot}s^{-1}$. After 1000 cycles of charge-discharge at a 10 $A{\cdot}g^{-1}$, it remained 92 % of the initial capacitance. The good capacitive was attributed to unique and outstanding structure of PGR and natural excellent pseudcapacitance of PANI. This work provided a new route for preparation of hybrid materials with remarkable pseudcapacitance for production of high-performance SCs.

Acknowledgments

This work was supported by the National Nature Science Foundation of China (No. 51672162), the Open Project Program of Key Laboratory for Analytical Science of Food Safety and Biology, Ministry of Education (FS18010), and the Fundamental Research Funds of Shandong University (No.2017JC035).

Conflict of interest

The authors declare that they have no conflict of interest.

Reference

1 P. Yang, L. Ma, M. Gan, Y. Lei, X. Zhang, M. Jin and G. Fu, *J. Mater. Sci. - Mater. Electron.*, 2017, **28**, 7333–7342.
2 J. Yan, Q. Wang, T. Wei and Z. Fan, *Adv. Energy Mater.*, 2014, **4**, 1300816.
3 J. P. Cheng, J. Zhang and F. Liu, *RSC Adv.*, 2014, **4**, 38893–38917.
4 L. Dong, Z. Chen, D. Yang and H. Lu, *RSC Adv.*, 2013, **3**, 21183.
5 H. Chen, S. Zhou, M. Chen and L. Wu, *J. Mater. Chem. A*, 2012, **22**, 25207–25216.
6 S. Yu, D. Liu, S. Zhao, B. Bao, C. Jin, W. Huang, H. Chen and Z. Shen, *RSC Adv.*, 2015, **5**, 30943–30949.
7 H. Chen, L. Hu, Y. Yan, R. Che, M. Chen and L. Wu, *Adv. Energy Mater.*, 2013, **3**, 1636–1646.
8 H. Chen, L. Hu, M. Chen, Y. Yan and L. Wu, *Adv. Funct. Mater.*, 2014, **24**, 934–942.
9 H. Chen, S. Zhou and L. Wu, *ACS Appl. Mater. Interfaces*, 2014, **6**, 8621–8630.
10 K. Wang, H. Wu, Y. Meng and Z. Wei, *Small*, 2014, **10**, 14–31.
11 J. Cao, Y. Wang, J. Chen, X. Li, F.C. Walsh, J.-H. Ouyang, D. Jia and Y. Zhou, *J. Mater. Chem. A*, 2015, **3**, 14445–14457.
12 D. S. Dhawale, D. P. Dubal, V. S. Jamadade, R. R. Salunkhe and C. D. Lokhande, *Synth. Met.*, 2010, **160**, 519–522.
13 X.-M. Feng, R.-M. Li, Y.-W. Ma, R.-F. Chen, N.-E. Shi, Q.-L. Fan and W. Huang, *Adv. Funct. Mater.*, 2011, **21**, 2989–2996.
14 Z. Wei and W. Wan, *Adv. Mater.*, 2010, **14**, 1314–1317.
15 G. A. Snook, P. Kao and A. S. Best, *J. Power Sources*, 2011, **196**, 1–12.
16 H. Mi, X. Zhang, S. An, X. Ye and S. Yang, *Electrochem. Commun.*, 2007, **9**, 2859–2862.
17 M. Wu, G. A. Snook, V. Gupta, M. Shaffer, D. J. Fray and G. Z. Chen, *J. Mater. Chem.*, 2005, **15**, 2297.
18 S. R. Sivakkumar, W. J. Kim, J.-A. Choi, D. R. MacFarlane, M. Forsyth and D.-W. Kim, *J. Power Sources*, 2007, **171**, 1062–1068.
19 C. Meng, C. Liu, L. Chen, C. Hu and S. Fan, *Nano Lett.*, 2010, **10**, 4025–4031.
20 S.C. Canobre, D.A.L. Almeida, C. Polo Fonseca and S. Neves, *Electrochim. Acta*, 2009, **54**, 6383–6388.
21 C. Meng, C. Liu and S. Fan, *Electrochem. Commun.*, 2009, **11**, 186–189.
22 K.-S. Kim and S.-J. Park, *Electrochim. Acta*, 2011, **56**, 1629–1635.
23 H. Zhang, G. Cao, W. Wang, K. Yuan, B. Xu, W. Zhang, J. Cheng and Y. Yang, *Electrochim. Acta*, 2009, **54**, 1153–1159.
24 M. Yang, B. Cheng, H. Song and X. Chen, *Electrochim. Acta*, 2010, **55**, 7021–7027.
25 Y. Zhou, Z.-Y. Qin, L. Li, Y. Zhang, Y.-L. Wei, L.-F. Wang and M.-F. Zhu, *Electrochim. Acta*, 2010, **55**, 3904–3908.
26 Z.-Z. Zhu, G.-C. Wang and M.-Q. Sun, *Electrochim. Acta*, 2011, **56**, 1366–1372.
27 H. Talbi, P. E. Just and L. H. Dao, *J. Appl. Electrochem.*, 2003, **33**, 465–473.
28 M. J. Bleda-Martínez, E. Morallón and D. Cazorla-Amorós, *Electrochim. Acta.*, 2007, **52**, 4962–4968.
29 K. S. Ryu, Y.-G. Lee, K. M. Kim, Y. J. Park, Y.-S. Hong, X. Wu, M. G. Kang, N.-G. Park, R.Y. Song and J. M. Ko, *Synth. Met.*, 2005, **153**, 89–92.
30 M. A. J. Bleda-Martínez, C. Peng, S. Zhang, G. Z. Chen, E. Morallón and D. Cazorla-Amorós, *J. Electrochem. Soc.*, 2008, **155**, A672.
31 W.-C. Chen and T.-C. Wen, *J. Power Sources*, 2003, **117**, 273–282.
32 J. Hu, H. Wang and X. Huang, *Electrochim. Acta*, 2012, **74**, 98–104.
33 F. Chen, P. Liu and Q. Zhao, *Electrochim. Acta*, 2012, **76**, 62–68.
34 K.-S. Kim and S.-J. Park, *Electrochim. Acta*, 2011, **56**, 6547–6553.
35 C. Li and G. Shi, *Electrochim. Acta*, 2011, **56**, 10737–10743.
36 K. I. Bolotin, K. J. Sikes, Z. Jiang, M. Klima, G. Fudenberg, J. Hone, P. Kim and H. L. Stormer, *Solid State Commun.*, 2008, **146**, 351–355.
37 M. D. Stoller, S. J. Park, Y. W. Zhu, J. H. An and R. S. Ruoff, *Nano Lett.*, 2008, **8**, 3498–3502.
38 Y. Luo, D. Kong, Y. Jia, J. Luo, Y. Lu, D. Zhang, K. Qiu, C.M. Li and T. Yu, *RSC Adv.*, 2013, **3**, 5851–5859.
39 Q. Wu, Y. X. Xu, Z. Y. Yao, A. R. Liu and G. Q. Shi, *ACS Nano*, 2010, **4**, 1963–1970.
40 N. B. Trung, T. V. Tam, H. R. Kim, S. H. Hur, E. J. Kim and W. M. Choi, *Chem. Eng. J.*, 2014, **255**, 89–96.
41 L. Qian and L. Lu, *RSC Adv.*, 2014, **4**, 38273–38280.
42 L. Qian and L. Lu, *Colloids Surf., A*, 2015, **465**, 32–38.
43 D. E. stilwell and S. M. Park, *J. Electrochem. Soc.*, 1988, **135**, 2254–2262.
44 V. Srinivasan and J. W. Weidner, *J. Power Sources*, 2002, **108**, 15–20.
45 K. Zhang, L. L. Zhang, X. S. Zhao and J. Wu, *Chem. Mater.*, 2010, **22**, 1392–1401.
46 Q. Wu, Y. Xu, Z. Yao, A. Liu and G. Shi, *ACS Nano.*, 2010, **4**, 1963–1970.
47 L. Hu, J. Tu, S. Jiao, J. Hou, H. Zhu and D. J. Fray, *Phys. Chem. Chem. Phys.*, 2012, **14**, 15652–15656.
48 K.-W. Shen, F. Ran, Y.-T. Tan, X.-Q. Niu, H.-L. Fan, K. Yan, L.-B. Kong and L. Kang, *Synth. Met.*, 2015, **199**, 205–213.
49 K. Wang, P. Zhao, X. Zhou, H. Wu and Z. Wei, *J. Mater. Chem.*, 2011, **21**, 16373–16378.
50 L.-B. Kong, J. Zhang, J.-J. An, Y.-C. Luo and L. Kang, *J. Mater. Sci.*, 2008, **43**, 3664–3669.